Electronic Supplementary Information for

The Indanone N-H Type Excited-state Intramolecular Proton Transfer (ESIPT); The Observation of Mechanically Induced ESIPT Reaction

Jhu-Jyun You,[a,ξ] Yan-Ding Lin,[b,ξ] Chao-Hsien Hsu,[b] Jiun-Wei Hu,[a] Ying-Yi Tsai,[b] Hao-Ting Qu,[b] Kew-Yu Chen,*[,a] and Pi-Tai Chou*[,b]

Department of Chemical Engineering, Feng Chia University, 40724 Taichung, Taiwan

E-mail: kyuchen@fcu.edu.tw

Department of Chemistry, National Taiwan University, 10617 Taipei, Taiwan.

E-mail: chop@ntu.edu.tw.

Contents

Experimental section

Synthesis and Characterization. All solvents were distilled freshly according to standard procedure. Commercially available reagents were used without further purification unless otherwise stated. All reactions were monitored by TLC. Column chromatography was performed using silica gel from Merck (230−400 mesh). ^{1}H and ^{13}C NMR spectra were recorded on a Varian Unity 400 spectrometer at 400 and 100 MHz, respectively. Chemical shifts (δ) are recorded in parts per million (ppm) and coupling constants (*J*) are reported in Hertz (Hz). Mass spectra were recorded on a VG70-250S mass spectrometer. FT-IR spectra were measured with a Horiba FT-720 infrared spectrophotometer.

X-ray Structure Analysis. Single-crystal X-ray diffraction data were acquired on a Bruker SMART 1000CCD diffractometer using λ (Mo-Kα) radiation (λ = 0.71073 Å). The data collection was executed using

the SMART program. Cell refinement and data reduction were carried out with the SAINT program. The structure was determined using the SHELXTL/PC program and refined using full-matrix least squares. All non-hydrogen atoms were refined anisotropically, whereas hydrogen atoms were placed at calculated positions and included in the final stage of refinements with fixed parameters. All crystal packing and molecular drawings were generated using Mercury software.[1] The CIF file of **1-4** have been deposited with the Cambridge Crystallographic Data Centre, having the associated deposition numbers 2371431-2371433, 2375635. A copy can be obtained free of charge on written application to CCDC, 12 Union Road, Cambridge, CB2 1EZ, UK (Fax: +44-12-2333-6033); on request via e-mail to deposit@ccdc.cam.uk or by access to http://www.ccdc.cam.ac.uk.

Computational Details. All the computational results were performed by the Gaussian 16 program. Geometries were optimized using the PBE0 functional,[2] the 6-311G** basis for compound **1-4**. The first excited-state structures were optimized by time-dependent DFT using the same hybrid functional. The absorption energies are calculated by the linear response approach under the corresponding ground state geometries.

Photophysical Properties. UV–visible absorption spectra were recorded on a UV–visible NIR spectrophotometer system (HITACHI UH5700). The steady-state emission spectra and excitation spectra were measured with a spectrofluorometer (Edinburgh FLS 980). Both the wavelength-dependent excitation and emission responses were calibrated. The emission QYs in solution were calculated using 2,2'-p-phenylene-bis(5-phenyloxazole) (POPOP) for compounds **1**, **3** normal-form and 4-(Dicyanomethylene)-2-methyl-6-(4-dimethylaminostyryl)-4*H*-pyran (DCM) for compounds **2**, **4**.

Time-Resolved Fluorescence Spectroscopy. The sub-nanosecond time-resolved measurement was carried out by a time-correlated single photon counting (TCSPC) system (OB-900, Edinburgh Instrument). Excitation light source was set up by the third harmonic generation (THG) of 900 nm light generated from the same femtosecond laser and giving 300 nm light source. The fluorescence of the sample was collected at an angle of 90o with respect to the pump beam. A polarizer, which is set at 54.7^{o} with respect to polarization of pump beam, was located on the light path of the pump beam in front of the detector to eliminate the anisotropy. The temporal resolution was estimated to be 15 ps after removing the instrument broadening. The ultrafast time-resolved spectroscopic studies were recorded by a FOG100 femtosecond up-conversion system (CDP) pumped by SHG of the same femtosecond pulse laser. In the experiment, the sample emission generated from a rotating sample cell and the interrogation gate pulse at designated delay time were focused on a BBO crystal with respect to the pump pulse for frequency summation. A l/2 plate was used to set polarization at magic angle of 54.7° between pump and gate pulse to avoid fluorescence anisotropy. The femtosecond time-resolved data were fitted to the sum of exponential functions convoluted with the IRF, which is fitted to 150 fs determined by Raman scattering signal.

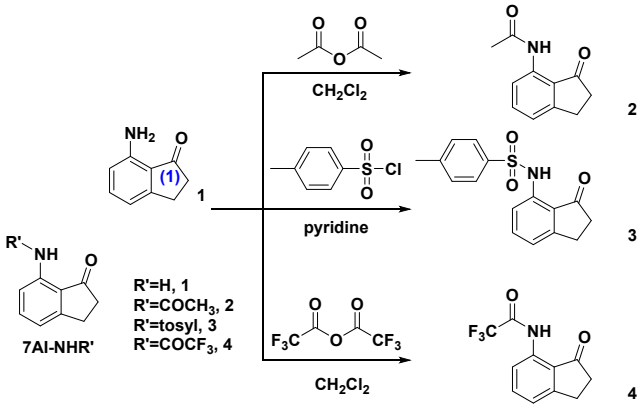

Scheme 1. The synthetic routes for the title compounds.

Synthesis of *N*-(3-oxo-2,3-dihydro-1*H*-inden-4-yl)acetamide (**2**). A mixture of 7-amino-1-indanone (**1**, 200 mg, 1.4 mmol) and acetic anhydride (0.22 mL, 2.0 mmol) in CH_2Cl_2 (15 mL) was stirred at room temperature for 3 h. After the solvent was removed, the crude product was purified by silica gel column chromatography with eluent ethyl acetate/*n*-hexane (1/4) to afford **3** (247 mg, 96%). ^{1}H NMR ($CDCl_3$, ppm) δ 10.39 (s, 1H), 8.37 (d, *J* = 8.0 Hz, 1H), 7.53 (t, *J* = 8.0 Hz, 1H), 7.08 (d, *J* = 8.0 Hz, 1H), 3.08 (t, *J* = 5.2 Hz, 2H), 2.70 (t, *J* = 5.2 Hz, 2H), 2.21 (s, 3H); ^{13}C NMR (100 MHz, $CDCl_3$, ppm)) δ 209.1, 169.4, 155.7, 138.6, 136.9, 122.5, 120.4, 116.5, 36.3, 25.2, 25.0; IR (KBr): 3291, 2938, 2860, 1671, 1574, 1508, 1450, 1404, 1360, 1231, 1165, 1024, 972, 785, 733 cm^{-1}; MS (EI, 70 eV): m/z (relative intensity) 189 (M^+, 100); HRMS calcd. for $C_{11}H_{11}NO_2$ 189.0790, found 189.0794. Colorless parallelepiped-shaped crystals suitable for the crystallographic studies reported here were isolated over a period of three weeks by slow evaporation from a dichloromethane solution.

Synthesis of 4-methyl-*N*-(3-oxo-2,3-dihydro-1*H*-inden-4-yl)benzenesulfonamide (**3**). A mixture of **1** (200 mg, 1.4 mmol) and tosyl chloride (290 mg, 1.5 mmol) in pyridine (10 mL) was stirred at room temperature for 12 h. Aqueous HCl was added and the mixture was extracted with CH_2Cl_2, and the combined organic layers were washed with water (3 times) and dried over Na_2SO_4 to yield the crude product. The crude product was purified by silica gel column chromatography with eluent ethyl acetate/n-hexane (1/3) to afford **2** (360 mg, 88 %). ^{1}H NMR ($CDCl_3$, ppm) δ 9.93 (s, 1H), 7.79 (d, *J* = 8.0 Hz, 2H), 7.41–7.42 (m, 2H), 7.21–7.23 (m, 2H), 7.02 (d, *J* = 8.0 Hz, 1H), 3.03 (t, *J* = 5.6 Hz, 2H), 2.66 (t, *J* = 5.6 Hz, 2H), 2.34 (s, 3H); ^{13}C NMR (100 MHz, $CDCl_3$, ppm) δ 208.5, 156.1, 144.0, 137.2, 136.3, 136.1, 129.6, 127.0, 122.8, 120.4, 113.9, 36.0, 25.2, 21.4; IR (KBr): 3175, 2952, 2853, 1680, 1640, 1576, 1530, 1462, 1410, 1280, 1244, 1183, 794, 706 cm^{-1}; MS (EI, 70 eV): m/z (relative intensity) 301 (M^+, 100); HRMS calcd. for $C_{16}H_{15}NO_3S$ 301.0773, found 301.0771. Colorless parallelepiped-shaped crystals suitable for the crystallographic studies reported here were isolated over a period of four weeks by slow evaporation from a dichloromethane solution.

Synthesis of 2,2,2-trifluoro-*N*-(3-oxo-2,3-dihydro-1*H*-inden-4-yl)acetamide (**4**). A mixture of **1** (200 mg, 1.4 mmol), trifluoroacetic anhydride (0.3 mL, 2.0 mmol) in CH_2Cl_2 (10 mL) was stirred at room temperature for 3 h. Saturated $NaHCO_3$(aq) was added and the mixture was extracted with ethyl acetate (3 x 10 mL). The combined organic extracts were dried over anhydrous Na_2SO_4, filtered, and concentrated under reduced

pressure. The crude product was purified by silica gel column chromatography with eluent ethyl acetate/*n*-hexane (1/4) to afford **4** (314 mg, 95%). ^{1}H NMR ($CDCl_3$, ppm) δ 11.30 (s, 1H), 8.20 (d, *J* = 8.0 Hz, 1H), 7.55 (t, *J* = 8.0 Hz, 1H), 7.22 (d, *J* = 8.0 Hz, 1H), 3.10 (t, *J* = 5.6 Hz, 2H), 2.70 (t, *J* = 5.6 Hz, 2H); ^{13}C NMR (100 MHz, $CDCl_3$, ppm) δ 209.0, 155.9, 155.0 (q, *J* = 37.5 Hz), 136.6, 135.4, 123.6, 122.8, 119.6 (q, *J* = 266.5 Hz), 116.7, 36.0, 25.3; IR (KBr): 3165, 2952, 2850, 1684, 1645, 1578, 1506, 1458, 1281, 1252, 995, 856, 799, 779 cm^{-1}; MS (EI, 70 eV): m/z (relative intensity) 243 (M^+, 100); HRMS calcd. for $C_{11}H_8F_3NO_2$ 243.0507, found 243.0503. Colorless parallelepiped-shaped crystals suitable for the crystallographic studies reported here were isolated over a period of four weeks by slow evaporation from a CH_2Cl_2 solution.

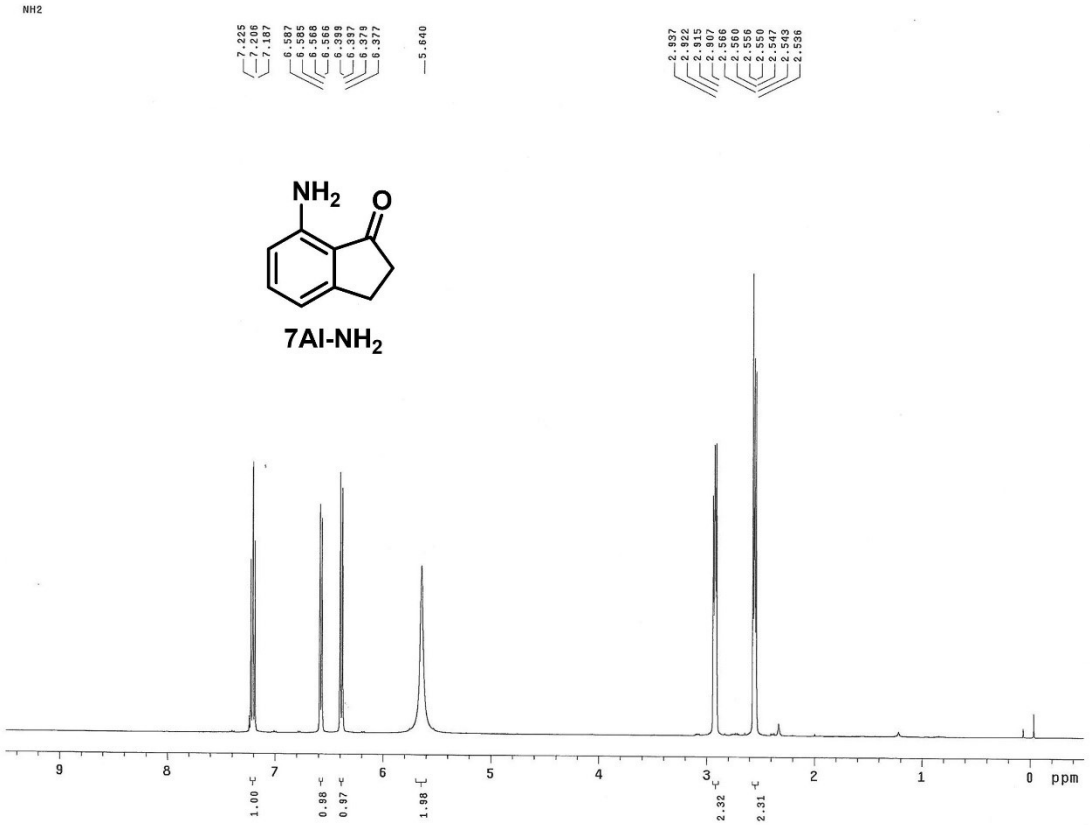

Figure S1. ^{1}H NMR spectrum of **1**.

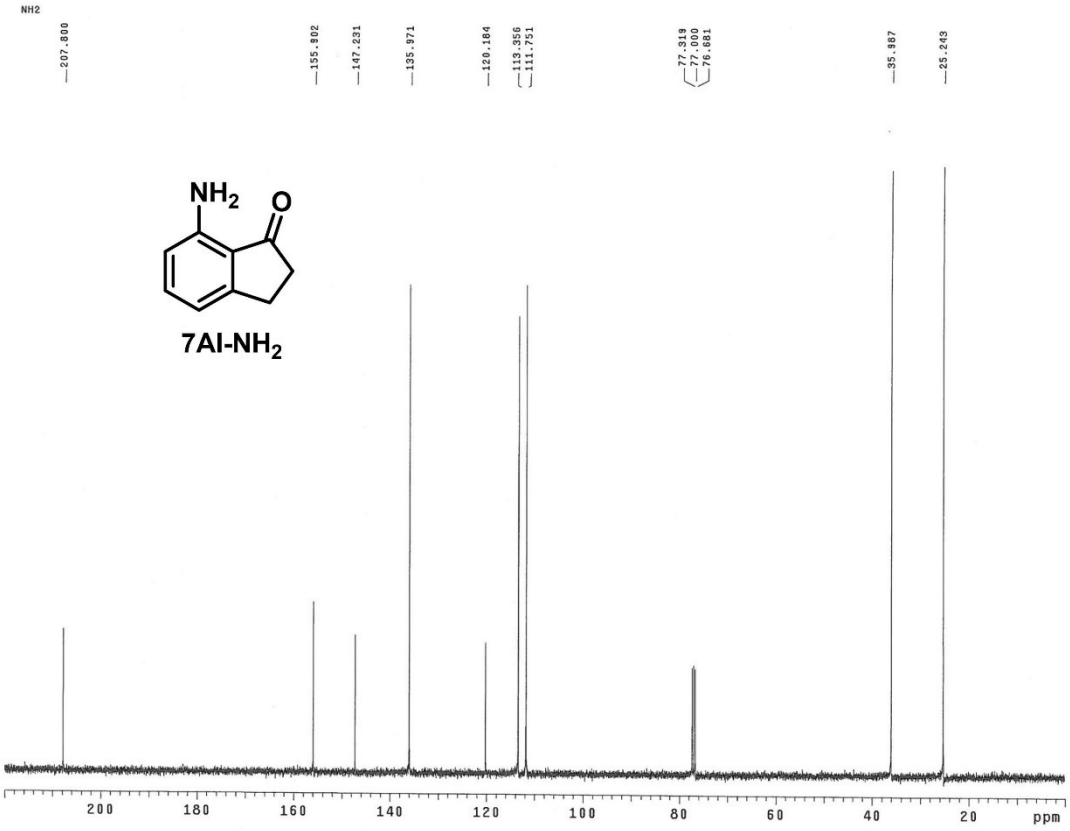

Figure S2. ^{13}C NMR spectrum of **1**.

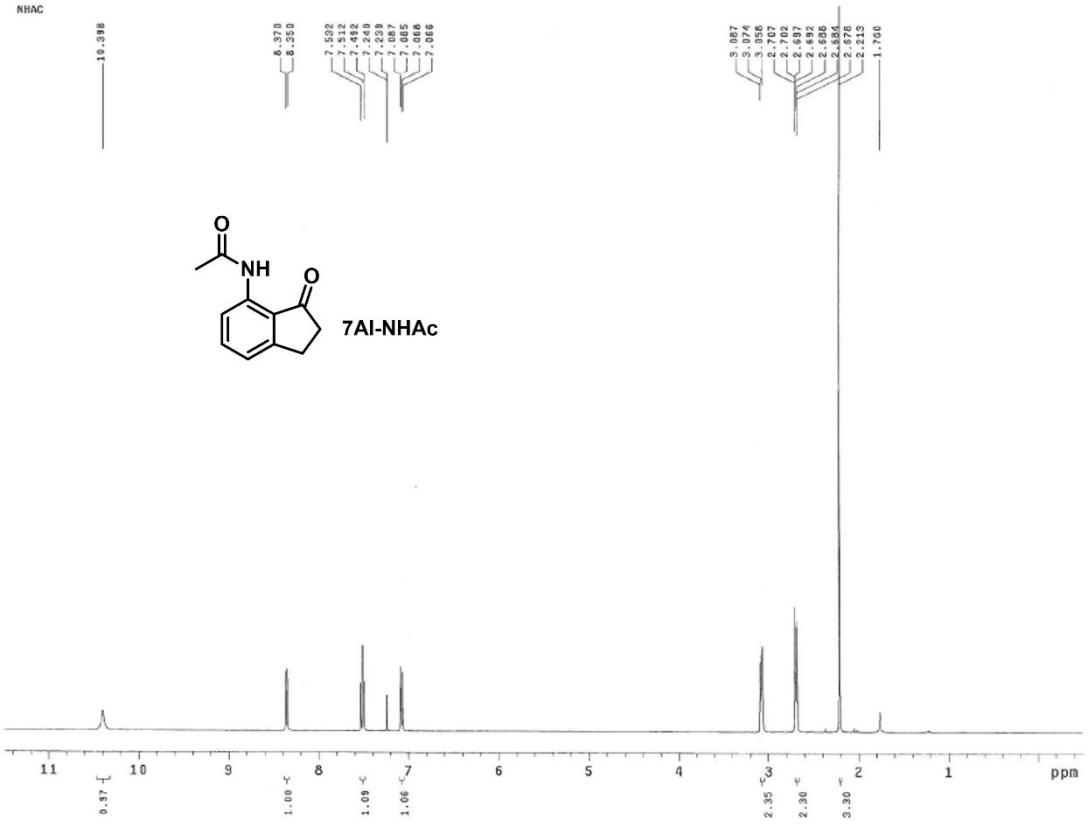

Figure S3. ^{1}H NMR spectrum of **2**.

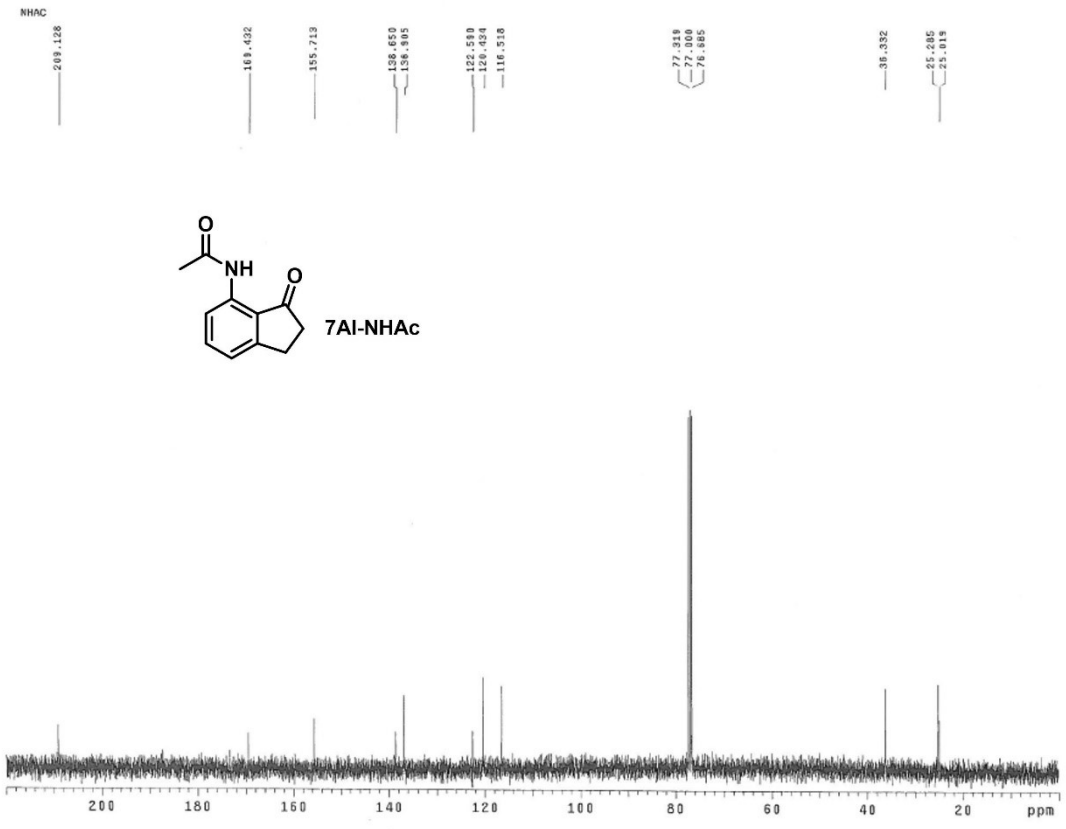

Figure S4. ^{13}C NMR spectrum of **2**.

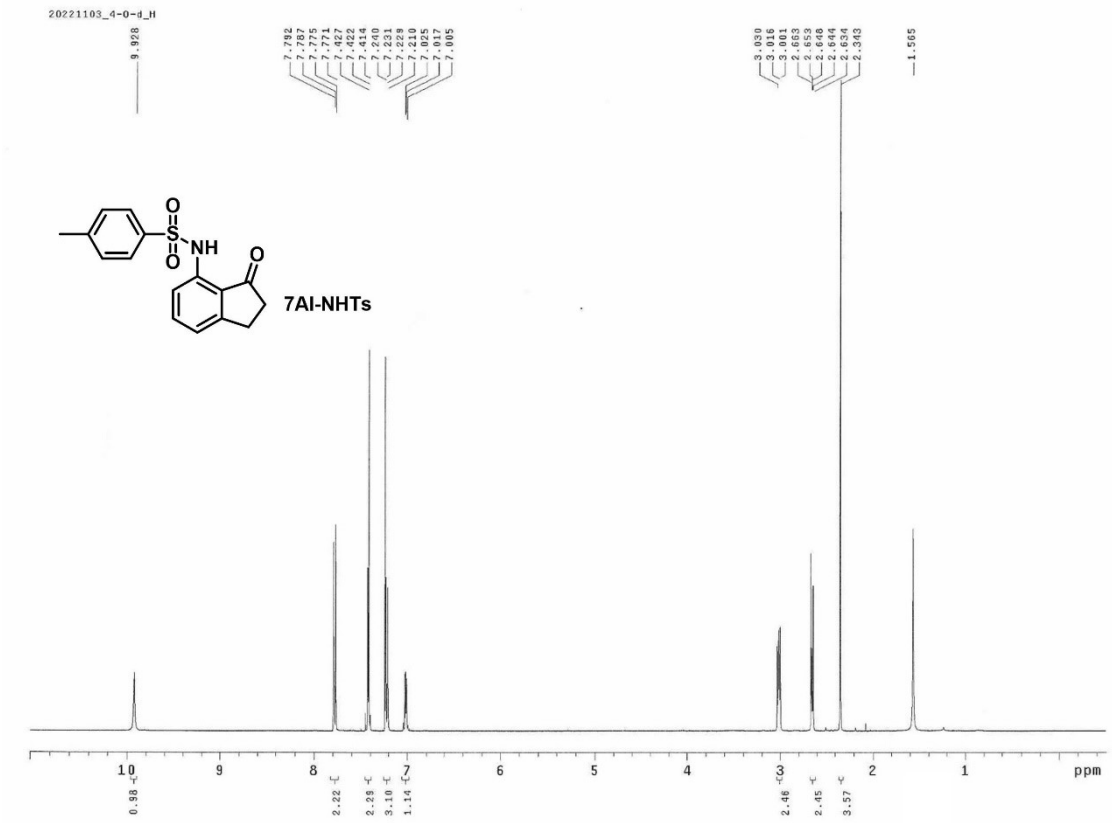

Figure S5. ^{1}H NMR spectrum of **3**.

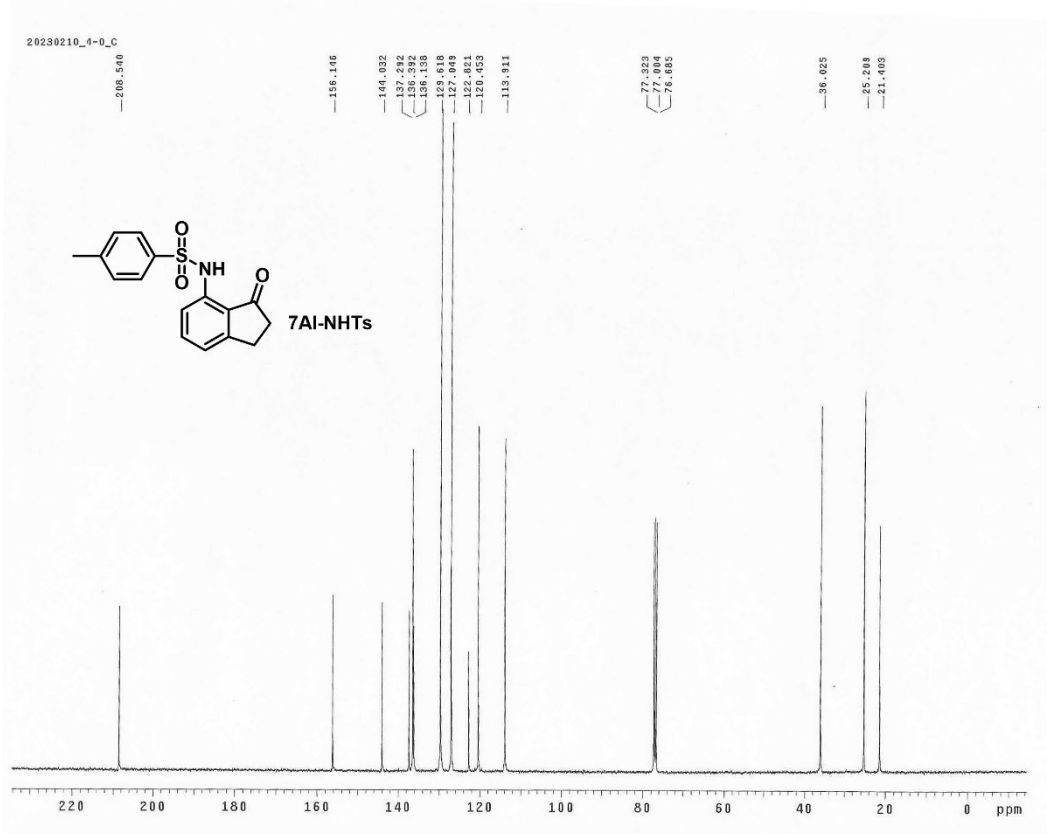

Figure S6. ^{13}C NMR spectrum of **3**.

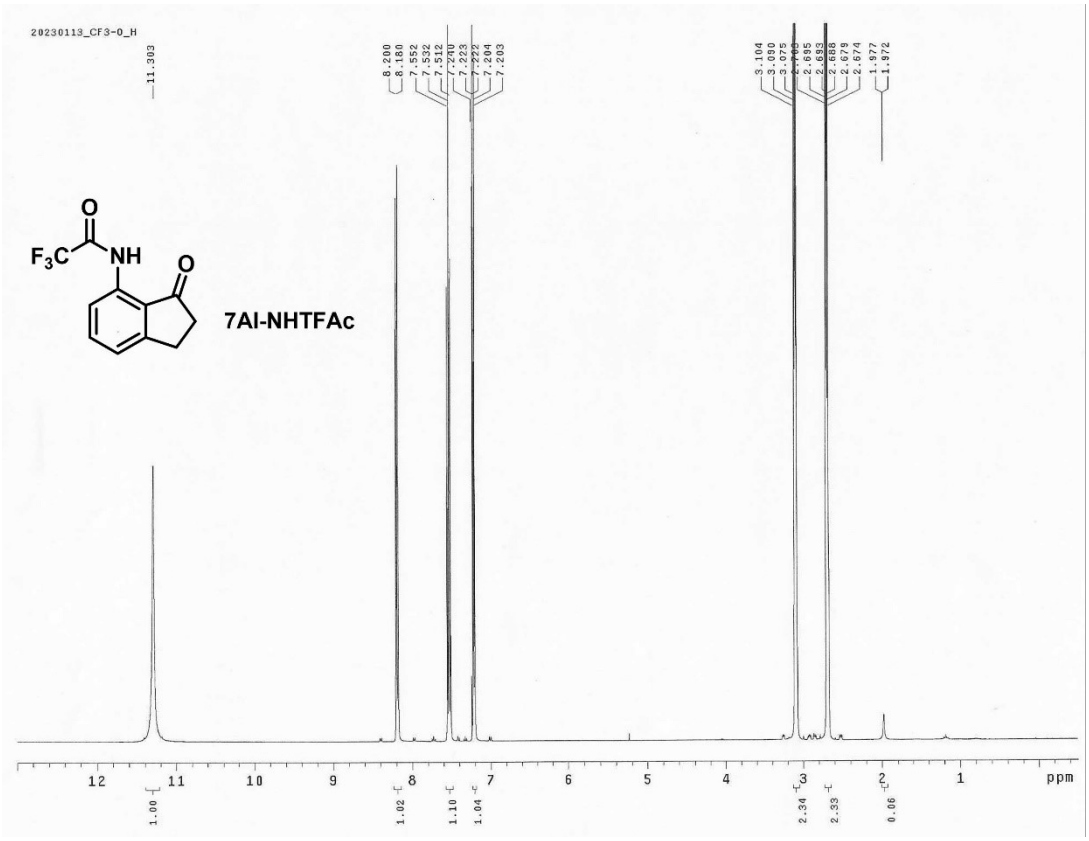

Figure S7. ^{1}H NMR spectrum of **4**.

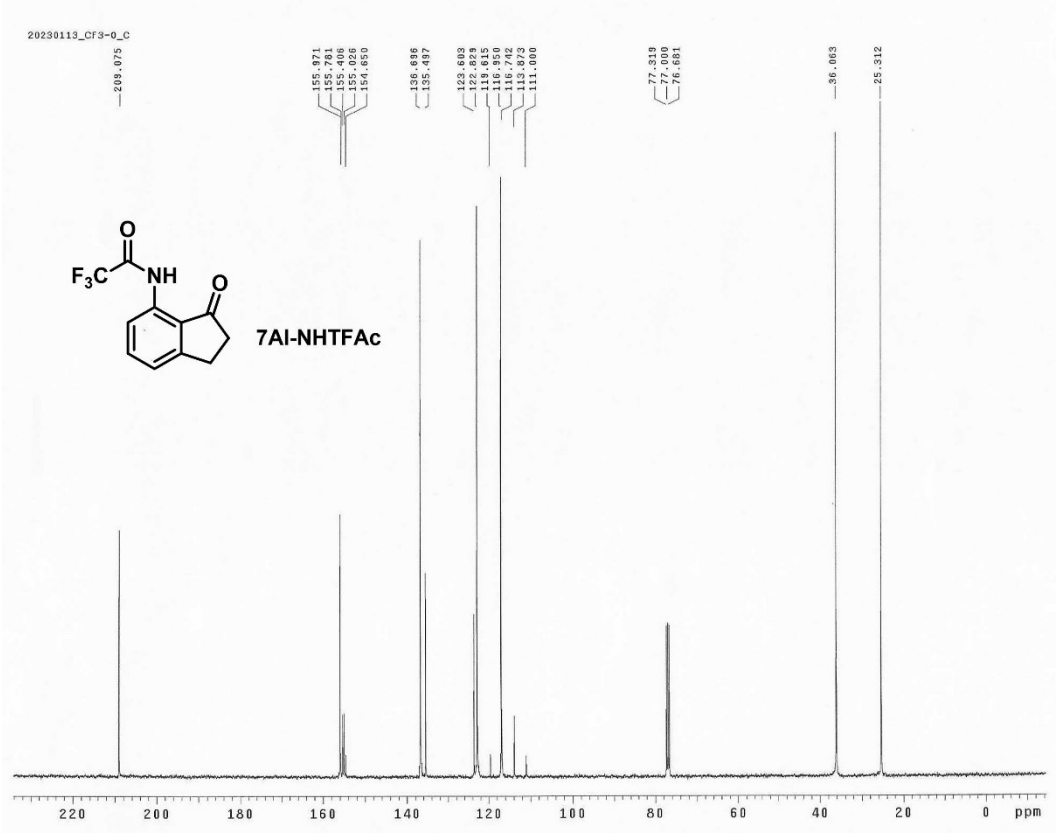

Figure S8. ^{13}C NMR spectrum of **4**.

Table S1. Crystal data and structure refinement for **1**.

Empirical formula	C_9H_9NO	
Formula weight	147.17	
Temperature	150(2) K	
Wavelength	0.71073 Å	
Crystal system	Tetragonal	
Space group	$I4_1/a$	
Unit cell dimensions	a = 19.9102(4) Å	α= 90°.
	b = 19.9102(4) Å	β= 90°.
	c = 7.2407(3) Å	γ= 90°.
Volume	2870.33(15) $Å^3$	
Z	16	
Density (calculated)	1.362 Mg/m^3	
Absorption coefficient	0.090 mm^{-1}	
F(000)	1248	
Crystal size	0.63 x 0.45 x 0.42 mm^3	
Theta range for data collection	2.894 to 29.047°.	
Index ranges	-26<=h<=26, -23<=k<=26, -7<=l<=9	
Reflections collected	10044	
Independent reflections	1787 [R(int) = 0.0428]	
Completeness to theta = 25.242°	99.9 %	
Absorption correction	Semi-empirical from equivalents	
Max. and min. transmission	1.00000 and 0.99306	
Refinement method	Full-matrix least-squares on F^2	
Data / restraints / parameters	1787 / 0 / 108	
Goodness-of-fit on F^2	1.065	
Final R indices [I>2sigma(I)]	R1 = 0.0471, wR2 = 0.1025	
R indices (all data)	R1 = 0.0655, wR2 = 0.1129	
Largest diff. peak and hole		0.218 and -0.245 $e.Å^{-3}$

Table S2. Crystal data and structure refinement for **2**.

Empirical formula	$C_{11}H_{11}NO_2$	
Formula weight	189.21	
Temperature	150(2) K	
Wavelength	0.71073 Å	
Crystal system	Monoclinic	
Space group	$P2_1/n$	
Unit cell dimensions	a = 7.2154(4) Å	α= 90°.
	b = 9.6795(6) Å	β= 97.728(2)°.
	c = 13.3482(9) Å	γ= 90°.
Volume	923.79(10) $Å^3$	
Z	4	
Density (calculated)	1.360 Mg/m^3	
Absorption coefficient	0.094 mm^{-1}	
F(000)	400	
Crystal size	0.470 x 0.170 x 0.130 mm^3	
Theta range for data collection	3.051 to 26.397°.	
Index ranges	-9<=h<=8, -12<=k<=12, -16<=l<=16	
Reflections collected	13495	
Independent reflections	1885 [R(int) = 0.0454]	
Completeness to theta = 25.242°	99.9 %	
Absorption correction	Semi-empirical from equivalents	
Max. and min. transmission	0.9281 and 0.8516	
Refinement method	Full-matrix least-squares on F^2	
Data / restraints / parameters	1885 / 0 / 131	
Goodness-of-fit on F^2	1.039	
Final R indices [I>2sigma(I)]	R1 = 0.0564, wR2 = 0.1532	
R indices (all data)	R1 = 0.0709, wR2 = 0.1640	
Largest diff. peak and hole	0.585 and -0.620 $e.Å^{-3}$	

Table S3. Crystal data and structure refinement for **3**.

Empirical formula	$C_{16}H_{15}NO_3S$	
Formula weight	301.35	
Temperature	150(2) K	
Wavelength	0.71073 Å	
Crystal system	Triclinic	
Space group	$P\bar{1}$	
Unit cell dimensions	a = 8.2512(5) Å	α= 64.7845(19)°.
	b = 13.5879(7) Å	β= 89.569(2)°.
	c = 14.6359(9) Å	γ= 75.610(2)°.
Volume	1428.91(15) $Å^3$	
Z	4	
Density (calculated)	1.401 Mg/m^3	
Absorption coefficient	0.236 mm^{-1}	
F(000)	632	
Crystal size	0.470 x 0.350 x 0.270 mm^3	
Theta range for data collection	2.565 to 27.911°.	
Index ranges	-10<=h<=10, -17<=k<=17, -19<=l<=19	
Reflections collected	41261	
Independent reflections	6814 [R(int) = 0.0347]	
Completeness to theta = 25.242°	99.8 %	
Absorption correction	Semi-empirical from equivalents	
Max. and min. transmission	0.7456 and 0.7003	
Refinement method	Full-matrix least-squares on F^2	
Data / restraints / parameters	6814 / 0 / 387	
Goodness-of-fit on F^2	1.034	
Final R indices [I>2sigma(I)]	R1 = 0.0423, wR2 = 0.1214	
R indices (all data)	R1 = 0.0510, wR2 = 0.1286	
Largest diff. peak and hole	0.484 and -0.468 e.$Å^{-3}$	

Table S4. Crystal data and structure refinement for **4**.

Empirical formula	$C_{11}H_8F_3NO_2$	
Formula weight	243.18	
Temperature	150(2) K	
Wavelength	0.71073 Å	
Crystal system	Monoclinic	
Space group	$P2_1$	
Unit cell dimensions	a = 7.4584(11) Å	α= 90°.
	b = 9.7135(15) Å	β= 91.033(6)°.
	c = 14.139(2) Å	γ= 90°.
Volume	1024.1(3) $Å^3$	
Z	4	
Density (calculated)	1.577 Mg/m^3	
Absorption coefficient	0.145 mm^{-1}	
F(000)	496	
Crystal size	0.490 x 0.220 x 0.110 mm^3	
Theta range for data collection	2.731 to 27.697°.	
Index ranges	-8<=h<=9, -12<=k<=12, -18<=l<=18	
Reflections collected	34372	
Independent reflections	4756 [R(int) = 0.0463]	
Completeness to theta = 25.242°	99.7 %	
Absorption correction	Semi-empirical from equivalents	
Max. and min. transmission	0.7456 and 0.6389	
Refinement method	Full-matrix least-squares on F^2	
Data / restraints / parameters	4756 / 1 / 309	
Goodness-of-fit on F^2	1.161	
Final R indices [I>2sigma(I)]	R1 = 0.0763, wR2 = 0.3030	
R indices (all data)	R1 = 0.0838, wR2 = 0.2073	
Absolute structure parameter	0.0(2)	
Largest diff. peak and hole	0.543 and -0.433 $e.Å^{-3}$	

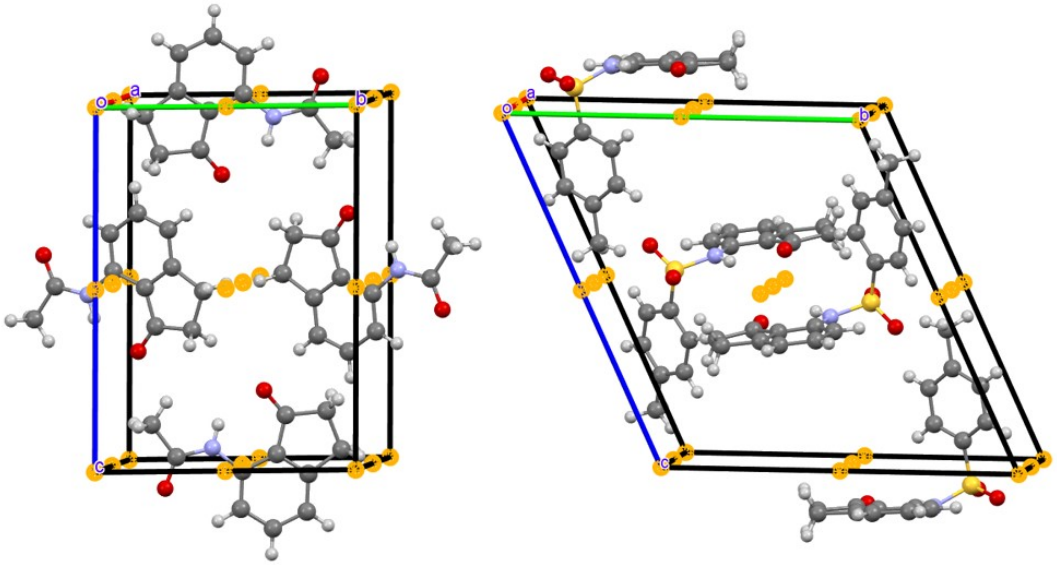

Compound **2**, space group: $P2_1/n$ centrosymmetric

Compound **3**, space group: $P\bar{1}$ centrosymmetric

Figure S9. Crystal packing structures of **2** (left) and **3** (right) where **2** and **3** are in a centrosymmetric arrangement (the inversion point is denoted by an orange dot).

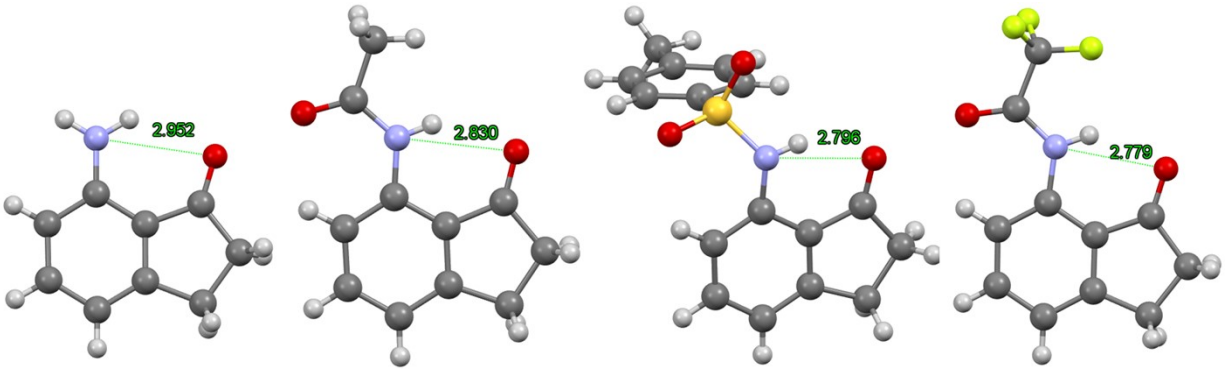

Figure S10. Single crystal structure of (a) **1**, (b) **2**, (c) **3**, and (d) **4**, green dash line denotes as N—O=C distances (Å).

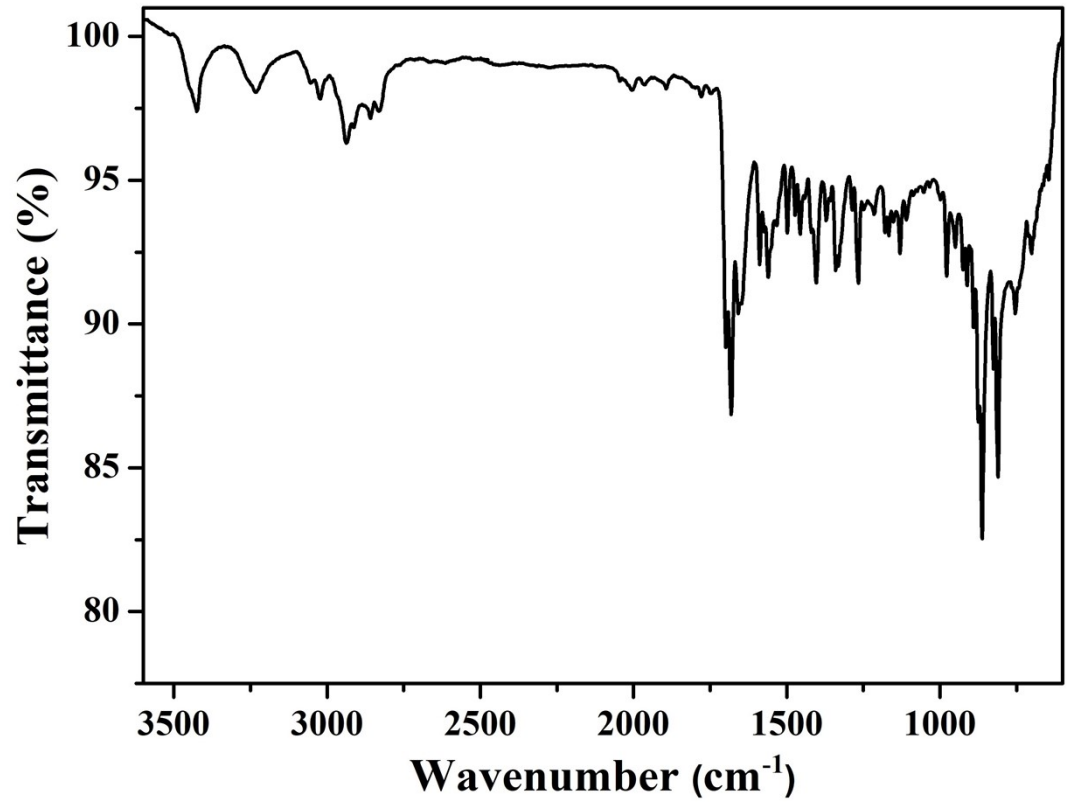

Figure S11. IR spectrum of **1**.

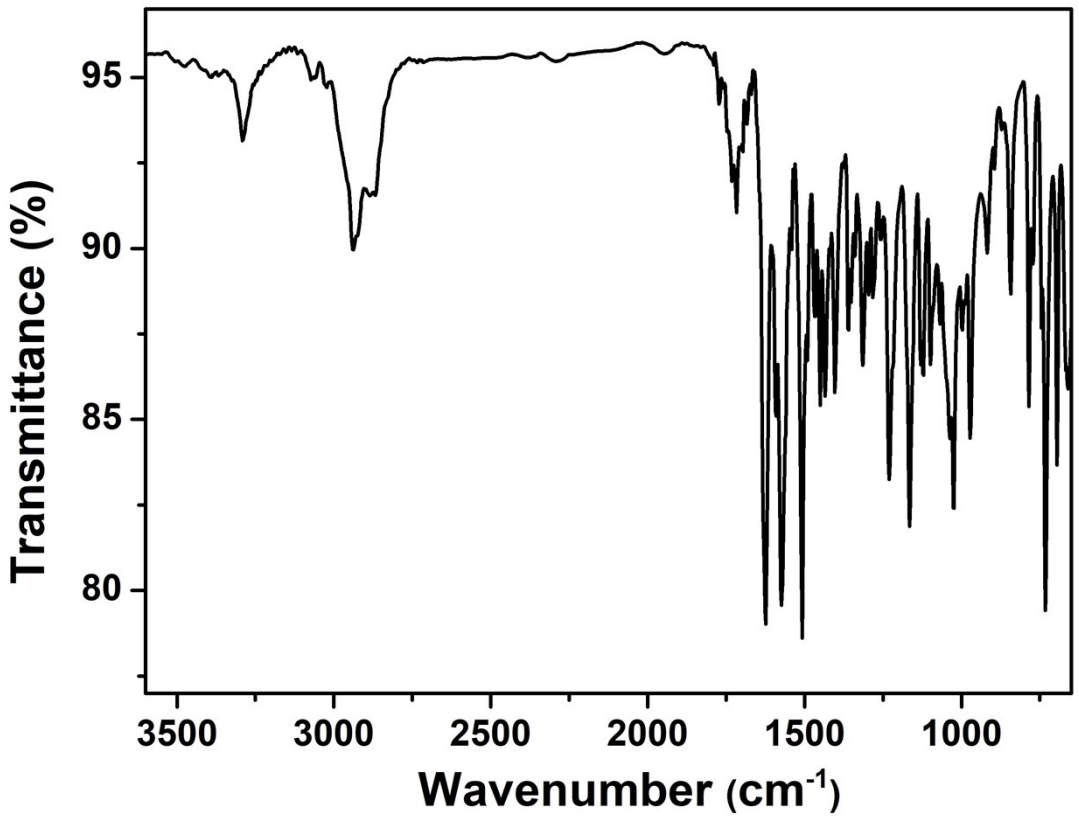

Figure S12. IR spectrum of **2**.

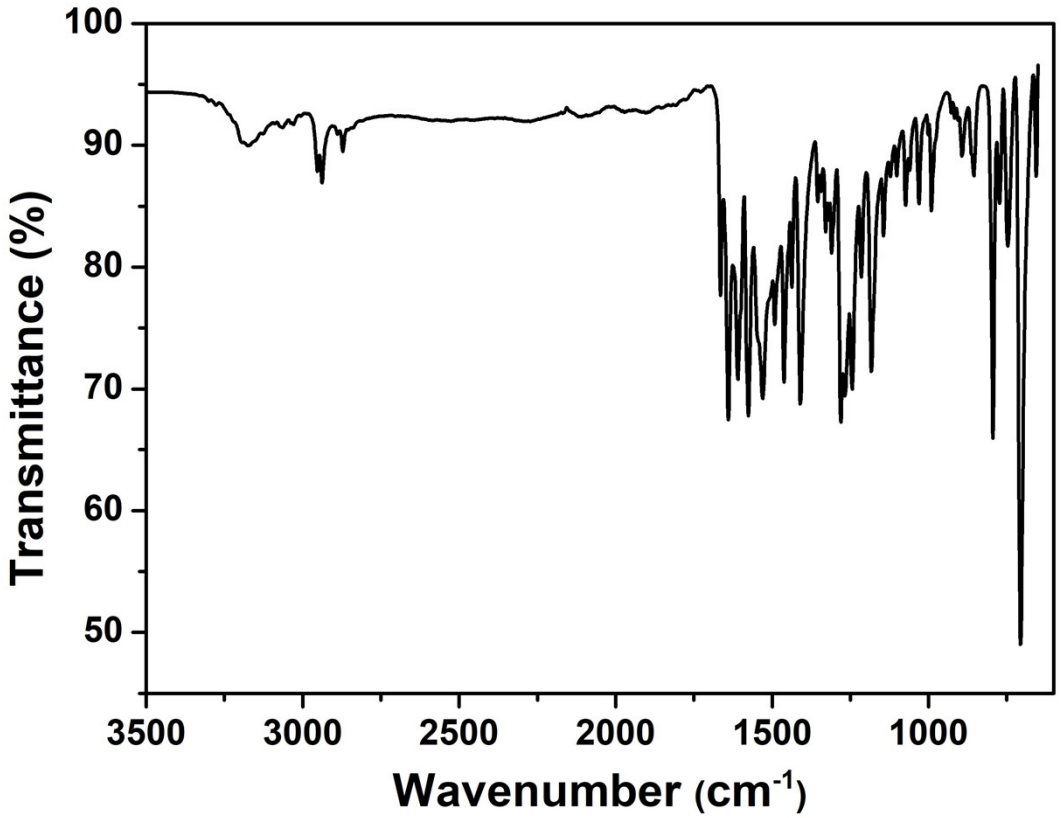

Figure S13. IR spectrum of **3**.

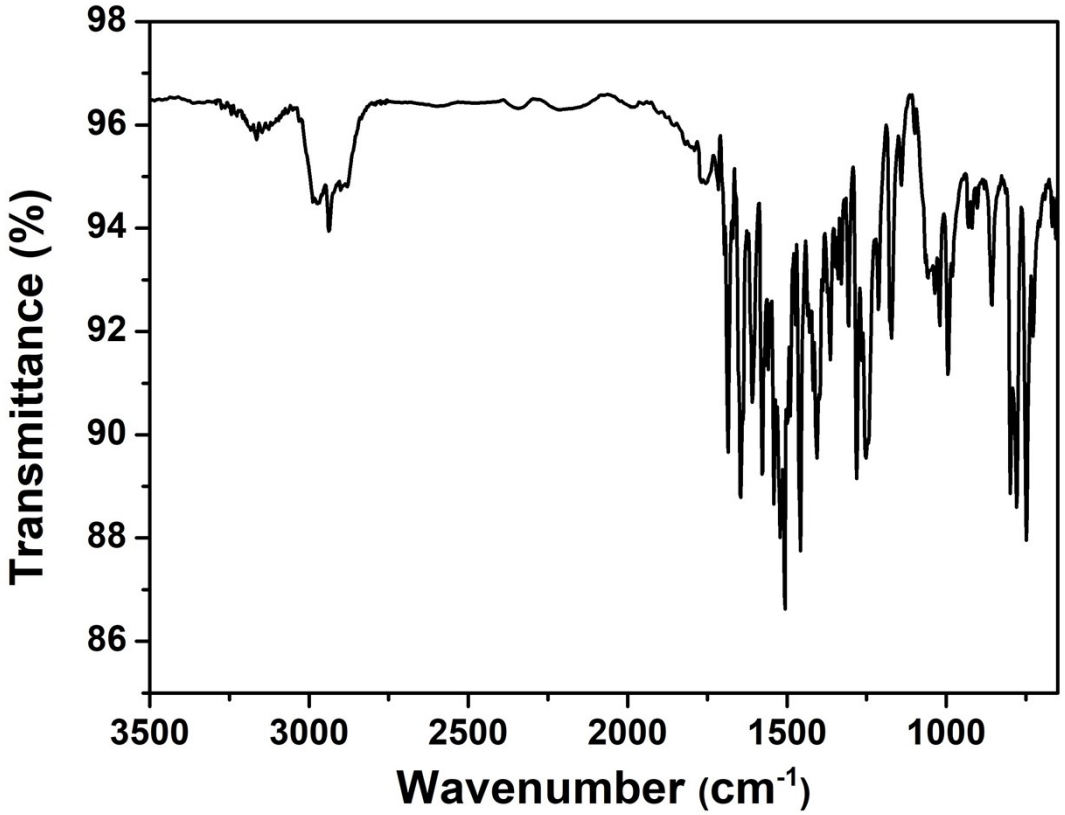

Figure S14. IR spectrum of **4**.

Table S5. Calculated excited-state characteristics of **1**-**4** in cyclohexane under PBE0/6-311+g(d,p).

Compound	λ_{abs} (S_1)[a] /nm	λ_{em} (S_1)[b] /nm	f_{em} (S_1)[c]	λ_{em} (S_1')[b] /nm	f_{em} (S_1')[c]	HOMO[d] /eV	LUMO[d] /eV	$\Delta E_{T^*\text{-}N^*}$ /eV
1	320	357	0.1215	488	0.1661	-5.98	-1.64	0.31
2	339	408	0.0014	491	0.1566	-7.01	-2.34	-0.04
3	339	376	0.0026	495	0.1631	-7.12	-2.38	-0.29
4	314	403	0.0005	491	0.1526	-7.28	-2.52	-0.52

[a] The absorption wavelength. [b] The emission wavelength. [c] Oscillator strength. [d] The energy level of HOMO and LUMO @S_1. Note: the ground state and the lowest lying excited state are denoted by S_0 and S_1, and S_0' and S_1' for normal and tautomer forms, respectively. Minor discrepancies in theoretical calculations do not compromise the reliability of the observed trends, which remain robust and consistent for accurate system interpretation.

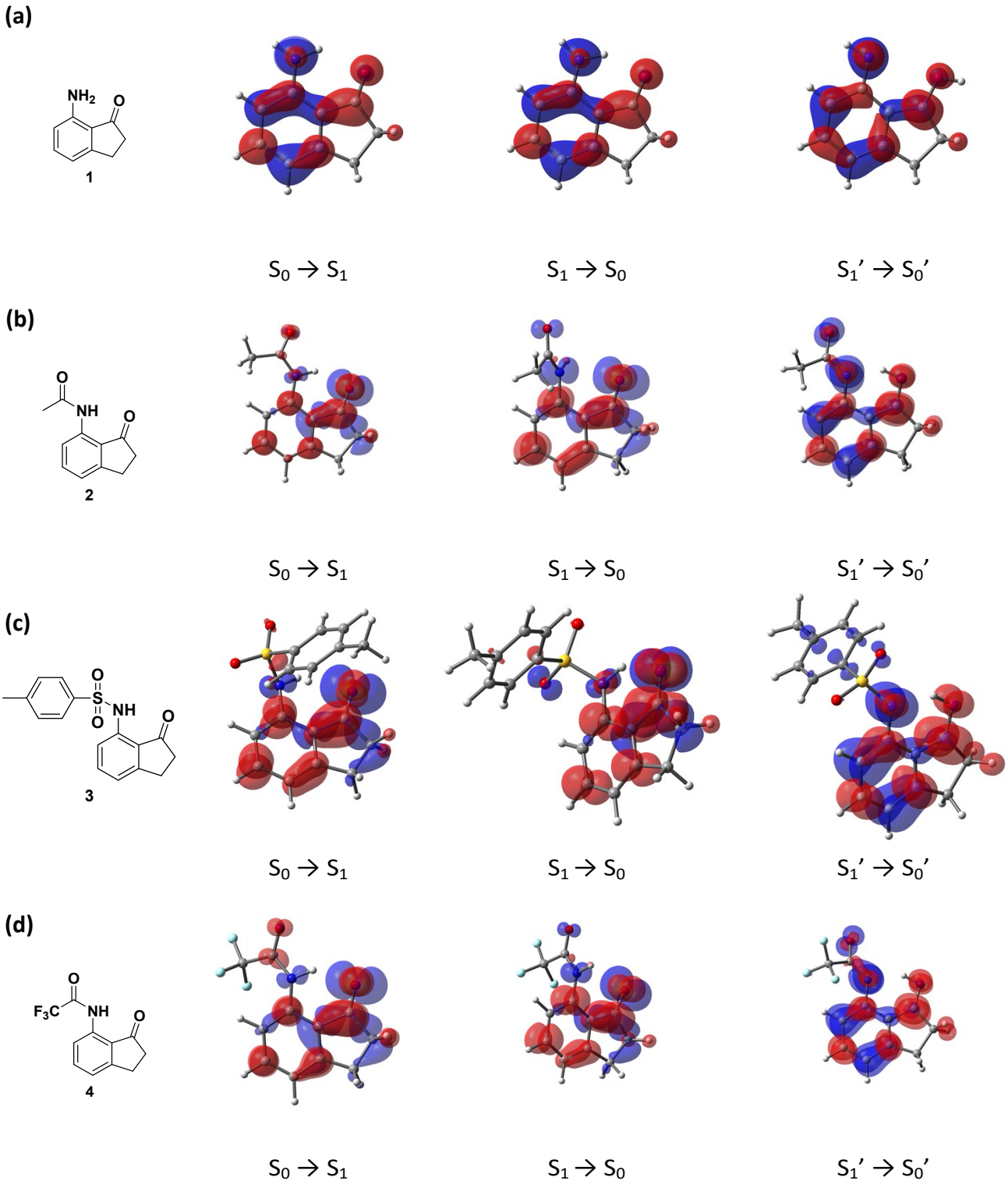

Figure S15. Excitation and emission electron density difference plots for (a) **1**, (b) **2**, (c) **3**, and (d) **4** (isovalue 0.002 a.u.). During the electronic transition, the electron density decreases in the blue areas and increases in the red areas. Note: the ground state and the lowest lying excited state are denoted by S_0 and S_1, and S_0' and S_1' for normal and tautomer forms, respectively.

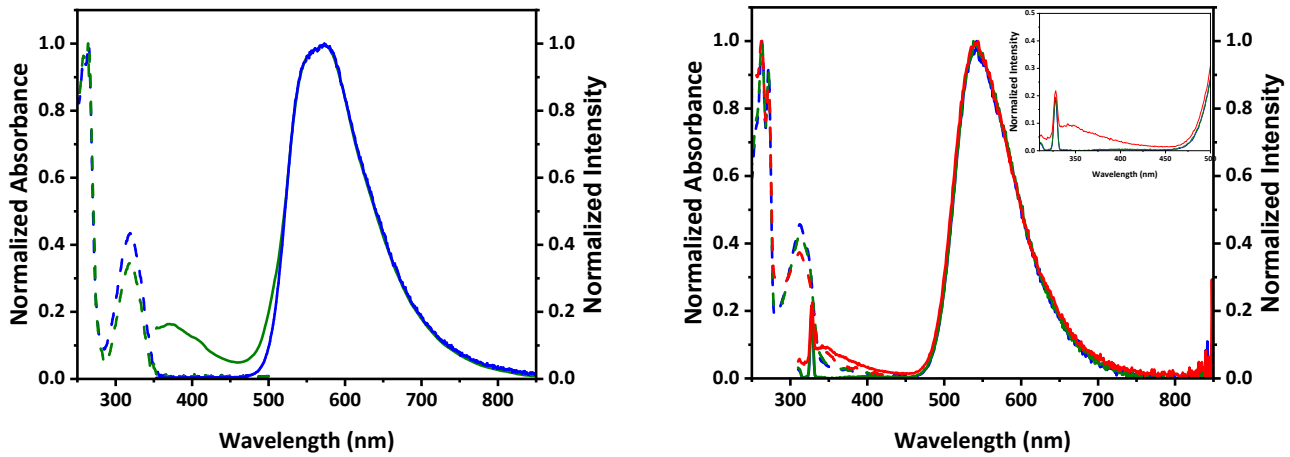

Figure S16. The absorption (dashed line) and emission (solid line) spectra of compound **3** (left) and **4** (right) in cyclohexane at 295 K with excitation at the absorption peak wavelength. The blue line represents 0 minutes of Xe lamp exposure, the green line represents 3 minute photolysis, and the red line represents 6 minute photolysis. The inset shows a magnified view of the impurity formation region. The Xe lamp used for excitation at 300 nm had a power of approximately 270 µW.

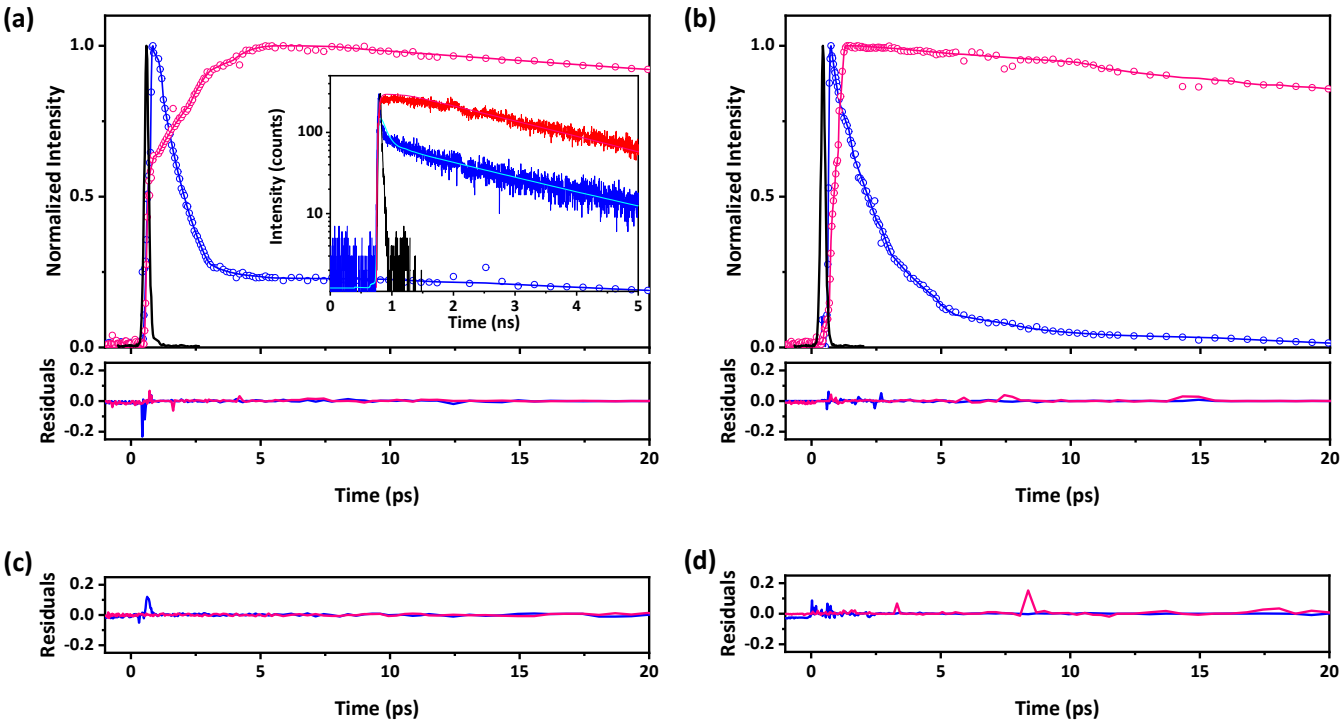

Figure S17. Presents the fluorescence up-conversion lifetimes and corresponding residuals for (a) **2** and (b) **3** in cyclohexane, with data points (blue and red) obtained by monitoring emission wavelengths at 400 nm and 600 nm, respectively, along with the IRF (black line). Solid lines depict the best exponential fits and the instrument response function (IRF). Note that in (b), the ~2-5 ps decay monitored at 400 nm is due to the photo-product formed during the up-conversion measurement (please see Figure S16 and text). Additionally, panels (c) and (d) display only the residuals for compounds **1** and **4**, as their fluorescence up-conversion data are already presented in the main text (Fig. 4a, 4b).

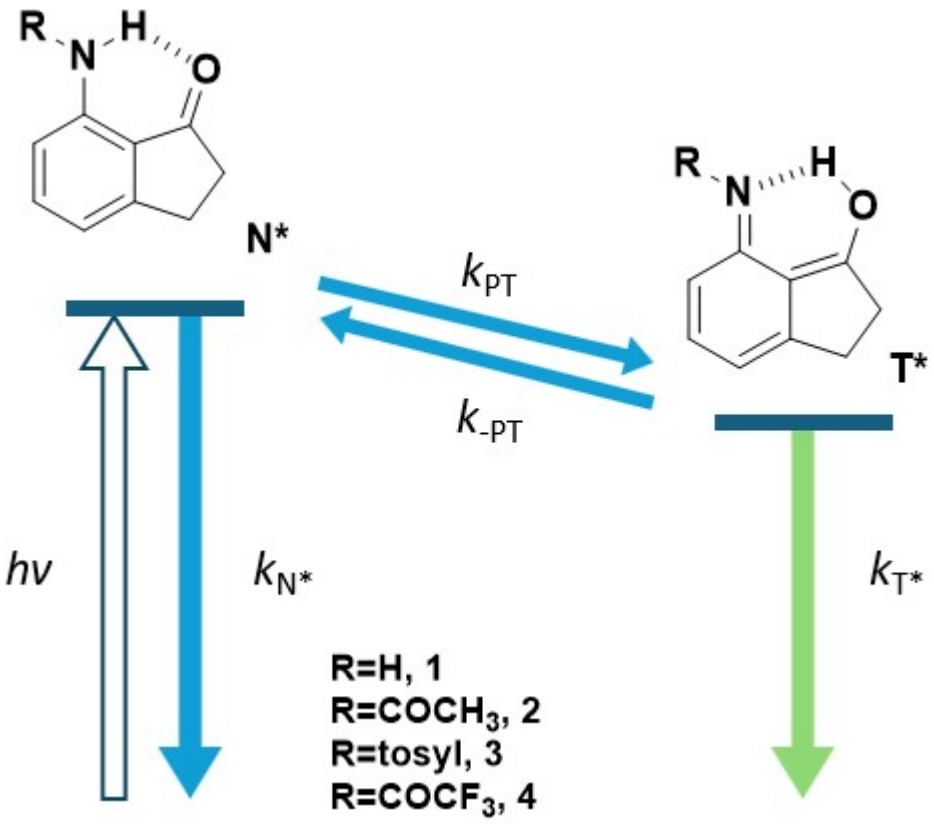

Scheme S1. Detail Kinetics Derivation of ESIPT Reaction. [N*]: concentration of normal species of excited state; [T*]: concentration of tautomer species of excited state; k_{pt}: proton transfer rate constant; k_{-pt}: reverse proton-transfer rate constant; k_{N*}: decay rate constant of N* for all decay channel except k_{pt}; k_{T*}: decay rate constant of T* for all decay channel except k_{-pt}

According to the reaction model shown in the Scheme S1, the differential rate equations for change of concentrations of normal and tautomer species can be expressed as follows:[3]

$$[N^*]_t = \frac{[N^*]_0}{\lambda_2 - \lambda_1} \times \left[(\lambda_2 - X) \times e^{-\lambda_1 t} + (X - \lambda_1) \times e^{-\lambda_2 t}\right] \quad (1)$$

$$[T^*]_t = \frac{k_{pt} \times [N^*]_0}{\lambda_2 - \lambda_1} \times \left[e^{-\lambda_1 t} - e^{-\lambda_2 t}\right] \quad (2)$$

Where, $\lambda_1 = \frac{(X+Y) - \sqrt{(X-Y)^2 + 4 \cdot k_{pt} \cdot k_{-pt}}}{2}$ and $\lambda_2 = \frac{(X+Y) + \sqrt{(X-Y)^2 + 4 \cdot k_{pt} \cdot k_{-pt}}}{2}$ With $X=k_{pt}+k_{N*}$ and $Y=k_{-pt}+k_{T*}$

When $[N^*]_t=[N^*]_0$ and $[T^*]_t=0$ at $t=0$, $X \approx k_{pt}$ and $Y \approx k_{-pt}$, Equation (3) can be derived.

$$\lambda_1 \cong \frac{k_{N*} + k_{T*} K_{eq}}{1 + K_{eq}};\ \lambda_2 = k_{pt} + k_{-pt} \qquad (3)$$

Accordingly, the pre-exponential factors that contribute to the fast and slow decay components of $[N^*]_t$, denoted as N_{fast} and N_{slow}, respectively, can be expressed by Equations (4) and (5).

$$N_{fast} \cong \frac{k_{pt}}{k_{pt} + k_{-pt}} \qquad (4)$$

$$N_{slow} \cong \frac{k_{-pt}}{k_{pt} + k_{-pt}} \qquad (5)$$

N_{fast} and N_{slow} can be obtained from the bi-exponential fitting of $[N^*]_t$ followed by extrapolation to t=0. The ratio of N_{fast} to N_{slow}, that is, $N_{fast}/N_{slow}=k_{pt}/k_{-pt}$, is equivalent to the pre-equilibrium constant K_{eq}.

Reference

1. C. F. Macrae, I. J. Bruno, J. A. Chisholm, P. R. Edgington, P. McCabe, E. Pidcock, L. Rodriguez-Monge, R. Taylor, J. Streek and P. A. Wood, *J. Appl. Crystallogr.*, 2008, **41**, 466-470.
2. M. Ernzerhof and G. E. Scuseria, *The Journal of Chemical Physics*, 1999, **110**, 5029-5036.
3. K.-C. Tang, M.-J. Chang, T.-Y. Lin, H.-A. Pan, T.-C. Fang, K.-Y. Chen, W.-Y. Hung, Y.-H. Hsu and P.-T. Chou, *Journal of the American Chemical Society*, 2011, **133**, 17738-17745.